Title:

III–V Light-Emitting Diodes on Silicon by Hydrogel-Mediated Wafer Bonding

Author Names:
Kosuke Nishigaya and Katsuaki Tanabe[z]

Affiliation:
Department of Chemical Engineering, Kyoto University, Nishikyo, Kyoto 615-8510, Japan

[z]Email: tanabe@cheme.kyoto-u.ac.jp

Abstract Text:

Monolithic on-chip integration of III–V compound semiconductor light-source components particularly on Si platforms is thought to be an important key technology in modern optoelectronics. Hydrogel-mediated semiconductor wafer bonding is an emerging technique for heterogeneous materials integration, simultaneously forming interfaces with high mechanical stability, electrical conductivity, optical transparency, and surface-roughness tolerance [K. Kishibe and K. Tanabe, *Appl. Phys. Lett.*, **115**, 081601 (2019)]. So far, its experimental demonstration has been limited to homogeneous Si/Si bonding and an application of solar-cell device. Here we demonstrate the fabrication and operation of a III–V light-emitting diode on Si, via heterogeneous GaAs/Si hydrogel-mediated wafer bonding. The bonding process is carried out in ambient air at room temperature, and therefore can potentially provide significant cost and throughput advantages in device production. Bonding with an unpolished back surface of semiconductor wafer with a micrometer-scale roughness is realized thanks to the deformability of hydrogel. The luminescence characteristics of the bonded device on Si are measured comparable to an unbonded reference. Stable operations of the device at over 70 ºC and for over 100 hours are demonstrated. Our experimental results verify the further suitability of the hydrogel-mediated semiconductor bonding scheme for optoelectronic device applications.

Introduction

Installation and integration of III–V compound semiconductor light-source components such as light-emitting diodes (LEDs) [1–5] and laser diodes [6–11] on Si is of a significant importance in the field of optoelectronics. Semiconductor wafer bonding [12–19] is a versatile fabrication method, widely used in optoelectronics. The bonding technique is able to form heterostructures of dissimilar semiconductor materials with high crystalline qualities, while the conventional epitaxial growth method inevitably generates substantial levels of defect densities due to crystalline lattice mismatches [20–23]. Therefore, wafer bonding is a promising scheme for high-performance semiconductor optoelectronics, and has been employed in the fabrication of a variety of devices such as light-emitting diodes [1,2,4,5,24], lasers [7,8,25–27], photodetectors [28,29], and solar cells [25,30–34]. Hydrogel-mediated semiconductor wafer bonding is an emerging technique for heterogeneous materials integration, simultaneously forming interfaces with high mechanical stability, electrical conductivity, optical transparency, and surface-roughness tolerance [35]. This hydrogel-mediated bonding technique has been applied to introduce wavelength-converting materials [36] and graphene quantum dots [37] into semiconductor interfaces, towards the realization of ultrahigh-performance optoelectronic devices. However, so far, the semiconductor material combination and device demonstration for hydrogel-mediated bonding have been limited to homogeneous Si-to-Si and a solar cell, respectively [35]. Therefore, the demonstration of a hydrogel-bonded light-emitting device would be an important technical milestone to verify the versatility of the hydrogel-mediated semiconductor bonding scheme for applications in optoelectronics. In addition, wafer bonding has recently been intensively employed for the implementation, integration, and performance improvement of various kinds of LEDs [38–42], and thus the bonding method is positioned as an essential manufacturing component for the near-future LED industry. In the present study, we demonstrate the fabrication and operation of a III–V LED on Si, via GaAs-to-Si heterogeneous hydrogel-mediated wafer bonding.

Experimental

The III–V LED structure, commonly employed for visible red emission [43,44], was epitaxially grown on a single-side-polished *p*-type GaAs <100> substrate with a thickness of 350 μm. The LED structure comprised, from the bottom to the top or in the growth sequence, a 100-nm-thick *p*-type GaAs layer, a 400-nm-thick *p*-type GaInP layer, an 80-nm-thick *p*-type GaAs layer, a 4-μm-thick *p*-type AlGaInP layer, a 700-nm-thick AlGaInP-based multiple-quantum-well layer, a 1-μm-thick *n*-type AlGaInP layer, and a 4.2-μm-thick *n*-type GaP layer. As the Si substrate, we used an epi-ready-grade, single-side-polished *p*-type Si wafer (thickness: 280 μm, crystalline plane orientation: <100>, dopant: boron, doping concentration: ~ 1×10^{19} cm^{-3}).

We performed the bonding process in a non-cleanroom, regular experimental room with a particle density of approximately 5 million m^{-3}, which we measured with a regular particle counter. The LED and Si wafers were diced into 0.64-cm^2 pieces. The Si piece was then subject to a wet hydrofluoric (HF) treatment (10% aq, 1 min) to remove the SiO_2 native oxide layer formed on the Si surface. As the hydrogel material, a 2.5-w/v% polyacrylamide (PAM) aq. was prepared via mixing PAM powder with deionized water and sufficiently stirring to

prevent the aggregation of the adhesive PAM particles. The prepared hydrogel was uniformly spin-coated onto the polished-side surface of the Si piece. The hydrogel-coated Si piece was then bonded to the unpolished back surface of the GaAs substrate of the LED piece under a uniaxial pressure of 0.1 MPaG in ambient air at room temperature for 3 h.

A front grid contact on top of the LED structure and a bottom contact on the back of the Si substrate were formed with a Au/Au–Ge–Ni metal material. Metal electrodes comprising a Au–Ge–Ni alloy (80:10:10 wt:wt:wt) and pure Au with thicknesses of 30 and 150 nm, respectively, were sequentially deposited by thermal evaporation to both outer-side surfaces of the bonded piece. In this manner, Au/Au–Ge–Ni/GaP and Au/Au–Ge–Ni/Si contacts were formed. We did not apply any annealing for the contacts to prevent potential heating influences to the bonded interfacial characteristics. In this electrode configuration, the current passes through the bonded interface during the LED operation. Therefore, these LED fabrication and operation tests are suitable to evaluate the validity of the hydrogel-mediated bonding scheme for optoelectronic device applications. For comparison, we also prepared a pristine reference LED sample from the same LED wafer with the same top and bottom electrodes, which was not bonded with a Si substrate but was standing alone. Figure 1 depicts schematic cross-sectional structural diagrams of the bonded and reference LED samples.

Results and Discussion

Figure 2 shows a plane-view and a cross-sectional scanning microscope image of the unpolished back surface of the GaAs substrate of the LED wafer, which is to be bonded to the Si piece. In the plane-view image, a combinative roughness of macroscopic morphology and microscopic etch pits is clearly observed. In the cross-sectional image, the GaAs surface roughness to be bonded is observed as approximately 5 μm. Even for such a highly rough semiconductor surface, we succeeded in the fabrication and operation of the bonded LED device, as shown in the following sections. In this way, we experimentally demonstrated that the hydrogel provides the tolerance for the roughness of the surfaces to be bonded owing to the soft, deformable bonding agent, verifying one of the advantages of the hydrogel-mediated bonding scheme. This roughness-tolerance effect is important in application use because in many cases bonding surfaces generally exhibit a certain degree of roughness as those surfaces are typically top surfaces that have undergone some fabrication procedures such as chemical treatments, crystal growth, or micro/nano processes. It is also worth noting that our bonding process in this work was carried out in a non-cleanroom, regular experimental room, thus demonstrating the high particulates tolerance of the hydrogel-bonding scheme, in contrast to direct bonding and bonding mediated by solid-state materials.

Figure 3 presents a cross-sectional scanning microscope image of the bonded interface in the fabricated III–V LED on Si. The semiconductor pieces were firmly in contact with each other at a mechanical stability sufficient to endure the cleavage of the bonded pair sample, despite the large roughness of the unpolished back-side surface of the GaAs substrate. The detachment normal stress of the bonded interface was measured as 43 kPa. The employment of the hydrogel PAM enables bond formation at room temperature [35]. The hydrogen bonds stemming from PAM may cause the adhesion to the semiconductor surfaces [45,46]. More specifically, hydrogen bonds presumably form between the $-NH_2$ groups of PAM and the semiconductor surface terminated by -OH groups owing to the water contained in PAM [45].

The bonded interface is observed to have an interlayer of PAM thin film with an approximate thickness of 5 μm. This PAM interlayer thickness is comparable to or larger than the roughness of the unpolished GaAs surface and typical diameters of particles in a regular, non-cleanroom environment (< 3 μm). Therefore, even in the presence of such roughness or particles on wafers, hydrogel films change their own morphology to enclose the interfacial gap or particles, and result in roughness and particulate tolerances. Moreover, the epitaxially grown semiconductor top surface has generally much smaller roughness than the thickness of such hydrogel films, indicating that the hydrogel-mediated bonding scheme would likewise mitigate the smoothness requirements on the surface roughness, for example, of epitaxial semiconductor materials to be bonded, to fabricate optoelectronic devices.

Figure 4 presents plane-view optical photographs of the bonded III–V LED on Si and the unbonded reference LED at a current density of 156 μA cm^{-2} (100 μA) at 25 ºC. As designated, clear light emission in the visible red region was observed for both of the samples. The emission intensity or brightness of the III–V LED on Si (Fig. 4a) was observed comparable to that of the reference unbonded LED (Fig. 4b). Figure 5 presents the light–voltage–current plots of the bonded III–V LED on Si and the unbonded reference LED at 25 ºC. The relatively high turn-on voltages for both of the bonded and reference LEDs are due to the non-ohmic, Schottky characteristics of the Au–Ge–Ni/GaP interface. The electrical series resistivity in the bonded LED was observed higher than that in the reference LED, presumably because of the existence of the bonded interface. The output optical power from the bonded LED was comparable to that from the reference LED at lower current densities, consistent with the observation in Fig. 4, but became lower at higher current densities. This difference in the output optical power could be potentially attributed to the larger temperature increase in the III–V multiple-quantum-well active region, which decreases the radiative recombination efficiency, in the bonded LED by Joule heating owing to the higher series resistance than the reference LED.

To evaluate the heating tolerance of the bonded LED device, we carried out the measurements at 73 ºC, which was the highest temperature our heating stage could reach. Figure 6 presents the light–current plots of the bonded III–V LED on Si at 25 and 73 ºC. Also plotted is the result for the second measurement run back at 25 ºC carried out after the measurement run at 73 ºC, to check the potential thermal degradation of the device. Seen in Fig. 6, the bonded LED device thus demonstrated its operation at a high temperature of 73 ºC. Remarkably, no thermal degradation of the bonded LED was observed at 73 ºC, represented by the comparable optical performance between the measurements at 25 ºC before and after the 73-ºC operation.

Figure 7 presents the luminescence spectra of the bonded III–V LED on Si and the unbonded reference LED at a current density of 781 μA cm^{-2} (500 μA) at 25 and 73 ºC. The LED emission peaks were positioned approximately at 625 nm, consistent with the luminescent color observed in Fig. 4, and 635 nm at 25 and 73 ºC, respectively, for both of the bonded and reference LEDs. The observed red-shift by the increase in the operation temperature could be attributed to the bandgap narrowing in the AlGaInP multiple quantum wells at higher temperature. The degree of the red-shift was observed larger for the bonded LED than for the reference LED. This difference could be attributed again to the larger temperature increase in the optical active region in the bonded LED by Joule heating owing

to the higher series resistance than that of the reference LED.

Finally we carried out a long-time operation test for the bonded III–V LED on Si, under a continuous current injection with a density of 25 μA cm^{-2} at 25 ºC. The resulted time-evolution of the output optical power from the bonded LED sample is presented in Fig. 8. As shown, the bonded device survived in the lifetime test over a hundred hours, with highly stable luminescence intensities. In addition, as observed in the inset of Fig. 8, the luminescence spectrum did not change during the measurement. Through the series of LED operation experiments in this work, the stability and suitability of the hydrogel-mediated semiconductor wafer bonding technique for optoelectronic device applications have thus been demonstrated.

Conclusions

In this work, we fabricated III–V light-emitting diodes on Si by using hydrogel-mediated semiconductor wafer bonding, and characterized the device performance. The bonding process was carried out in ambient air at room temperature, unlike in conventional growth methods and direct semiconductor bonding processes, thereby emphasizing significant cost and throughput advantages in device production. Bonding with a highly rough surface such as the unpolished back surface of the semiconductor wafers with a micrometer-scale roughness was realized owing to the deformability of hydrogel. The device characteristics of the bonded LED on Si were measured to be comparable to those of the unbonded pristine LED. However, the electrical conductivity and optical intensity for the bonded LED were lower than those for the reference LED at higher current densities. Therefore, improvement of the electrical conductivity in the bonded interface to suppress the heating effect is a future subject. Device operation tests at over 70 ºC and for over 100 h were conducted. The results demonstrated the validity of hydrogel-mediated semiconductor wafer bonding for applications in optoelectronics.

Acknowledgments

The authors would like to thank Akihiro Wakahara of Toyohashi University of Technology for his advice on the AlGaInP epitaxial wafer and Kodai Kishibe of Kyoto University for his technical support on the metal-electrode deposition equipment. This study was supported, in part, by the Murata Science Foundation and the Japan Society for the Promotion of Science (JSPS).

References

1. W. S. Wong, T. Sands, N. W. Cheung, M. Kneissl, D. P. Bour, P. Mei, L. T. Romano, and N. M. Johnson, *Appl. Phys. Lett.*, **77**, 2822 (2000).
2. S. -J. Lee, K. H. Kim, J. -W. Ju, T. Jeong, C. -R. Lee, and J. H. Baek, *Appl. Phys. Express*, **4**, 066501 (2011).
3. M. Rajesh, K. Tanabe, S. Kako, K. Kawaguchi, M. Nishioka, and Y. Arakawa, *Jpn. J. Appl. Phys.*, **53**, 04EH05 (2014).
4. K. Matsumoto, X. X. Zhang, J. Kishikawa, and K. Shimomura, *Jpn. J. Appl. Phys.*, **54**, 030208 (2015).
5. C. -M. Kang, J. -Y. Lee, D. -J. Kong, J. -P. Shim, S. -H. Kim, S. -H. Mun, S. -Y. Choi, M. -D. Park, J. Lee, and D. -S. Lee, *ACS Photon.*, **5**, 4413 (2018).
6. J. P. van der Ziel, R. D. Dupuis, and J. C. Bean, *Appl. Phys. Lett.*, **48**, 1713 (1986).
7. A. W. Fang, H. Park, O. Cohen, R. Jones, M. J. Paniccia, and J. E. Bowers, *Opt. Express*, **14**, 9203 (2006).
8. J. Van Campenhout, P. Rojo-Romeo, P. Regreny, C. Seassal, D. Van Thourhout, S. Verstuyft, L. Di Cioccio, J. M. Fedeli, C. Lagahe, and R. Baets, *Opt. Express*, **15**, 6744 (2007).
9. Z. Wang, B. Tian, M. Pantouvaki, W. Guo, P. Absil, J. Van Campenhout, C. Merckling, and D. Van Thourhout, *Nat. Photon.*, **9**, 837 (2015).
10. S. Chen, W. Li, J. Wu, Q. Jiang, M. Tang, S. Shutts, S. N. Elliott, A. Sobiesierski, A. J. Seeds, I. Ross, P. M. Smowton, and H. Liu, *Nat. Photon.*, **10**, 307 (2016).
11. Y. Sun, K. Zhou, Q. Sun, J. Liu, M. Feng, Z. Li, Y. Zhou, L. Zhang, D. Li, S. Zhang, M. Ikeda, S. Liu, and H. Yang, *Nat. Photon.*, **10**, 595 (2016).
12. J. B. Lasky, *Appl. Phys. Lett.*, **48**, 78 (1986).
13. M. Shimbo, K. Furukawa, K. Fukuda, and K. Tanzawa, *J. Appl. Phys.*, **60**, 2987 (1986).
14. Q. -Y. Tong, R. Gafiteanu, and U. Gösele, *J. Electrochem. Soc.*, **139**, L101 (1992).
15. K. Ljungberg, Y. Backlund, A. Soderbarg, M. Bergh, M. O. Andersson, and S. Bengtsson, *J. Electrochem. Soc.*, **142**, 1297 (1995).
16. O. Moutanabbir, *ECS Trans.*, **33**, 177 (2010).
17. L. Di Cioccio, P. Gueguen, R. Taibi, D. Landru, G. Gaudin, C. Chappaz, F. Rieutord, F. de Crecy, I. Radu, L. L. Chapelon, and L. Clavelier, *J. Electrochem. Soc.*, **158**, P81 (2011).
18. S. Essig and F. Dimroth, *ECS J. Solid State Sci. Technol.*, **2**, Q178 (2013).
19. R. Takigawa, T. Matsumae, M. Yamamoto, E. Higurashi, T. Asano, and H. Kanaya, *ECS J. Solid State Sci. Technol.*, **9**, 045005 (2020).
20. H. Kroemer, T. Y. Liu, and P. M. Petroff, *J. Cryst. Growth*, **95**, 96 (1989).
21. M. Sugo, Y. Takanashi, M. M. Al-Jassim, and M. Yamaguchi, *J. Appl. Phys.*, **68**, 540 (1990).
22. K. Samonji, H. Yonezu, Y. Takagi, K. Iwaki, N. Ohshima, J. K. Shin, and K. Pak, *Appl. Phys. Lett.*, **69**, 100 (1996).
23. J. Z. Li, J. Bai, J. S. Park, B. Adekore, K. Fox, M. Carroll, A. Lochtefeld, and Z. Shellenbarger, *Appl. Phys. Lett.*, **91**, 021114 (2007).
24. J. Chun, K. J. Lee, Y. C. Leem, W. M. Kang, T. Jeong, J. H. Baek, H. J. Lee, B. J. Kim,

and S. J. Park, *ACS Appl. Mater. Interfaces*, **6**, 19482 (2014).
25. K. Tanabe, K. Watanabe, and Y. Arakawa, *Sci. Rep.*, **2**, 349 (2012).
26. D. Liang, X. Huang, G. Kurczveil, M. Fiorentino, and R. G. Beausoleil, *Nat. Photon.*, **10**, 719 (2016).
27. G. Crosnier, D. Sanchez, S. Bouchoule, P. Monnier, G. Beaudoin, I. Sagnes, R. Raj, and F. Raineri, *Nat. Photon.*, **11**, 297 (2017).
28. H. Park, A. W. Fang, R. Jones, O. Cohen, O. Raday, M. N. Sysak, M. J. Paniccia, and J. E. Bowers, *Opt. Express*, **15**, 6044 (2007).
29. L. Chen, P. Dong, and M. Lipson, *Opt. Express*, **16**, 11513 (2008).
30. K. Tanabe, A. Fontcuberta i Morral, H. A. Atwater, D. J. Aiken, and M. W. Wanlass, *Appl. Phys. Lett.*, **89**, 102106 (2006).
31. F. Dimroth, M. Grave, P. Beutel, U. Fiedeler, C. Karcher, T. N. D. Tibbits, E. Oliva, G. Siefer, M. Schachtner, A. Wekkeli, A. W. Bett, R. Krause, M. Piccin, N. Blanc, C. Drazek, E. Guiot, B. Ghyselen, T. Salvetat, A. Tauzin, T. Signamarcheix, A. Dobrich, T. Hannappel, and K. Schwarzburg, *Prog. Photovolt.*, **22**, 227 (2014).
32. S. Essig, C. Allebé, T. Remo, J. F. Geisz, M. A. Steiner, K. Horowitz, L. Barraud, J. S. Ward, M. Schnabel, A. Descoeudres, D. L. Young, M. Woodhouse, M. Despeisse, C. Ballif, and A. Tamboli, *Nat. Energy*, **2**, 17144 (2017).
33. R. Cariou, J. Benick, F. Feldmann, O. Höhn, H. Hauser, P. Beutel, N. Razek, M. Wimplinger, B. Bläsi, D. Lackner, M. Hermle, G. Siefer, S. W. Glunz, A. W. Bett, and F. Dimroth, *Nat. Energy*, **3**, 326 (2018).
34. J. F. Geisz, R. M. France, K. L. Schulte, M. A. Steiner, A. G. Norman, H. L. Guthrey, M. R. Young, T. Song, and T. Moriarty, *Nat. Energy*, **5**, 326 (2020).
35. K. Kishibe and K. Tanabe, *Appl. Phys. Lett.*, **115**, 081601 (2019).
36. K. Kishibe, S. Hirata, R. Inoue, T. Yamashita, and K. Tanabe, *Nanomaterials*, **9**, 1742 (2019).
37. K. Nishigaya, K. Kishibe, and K. Tanabe, *C*, **6**, 28 (2020).
38. J. Chun, Y. Hwang, Y. -S. Choi, J. -J. Kim, T. Jeong, J. H. Baek, H. C. Ko, and S. -J. Park, *Scr. Mater.*, **77**, 13 (2014).
39. J. H. Choi, J. Kim, H. Yoo, J. Liu, S. Kim, C. -W. Baik, C. -R. Cho, J. G. Kang, M. Kim, P. V. Braun, S. Hwang, and T. -S. Jung, *Adv. Opt. Mater.*, **4**, 505 (2016).
40. M. -C. Tseng, D. -S. Wuu, C. -L. Chen, H. -Y. Lee, Y. -C. Lin, and R. -H. Horng, *Opt. Mater. Express*, **6**, 3293 (2016).
41. S. A. U. Hasan and H. Youn, *Nanoscale*, **9**, 9716 (2017).
42. M. Ichikawa, T. Kemmochi, T. Mukai, M. Uomoto, and T. Shimatsu, *ECS J. Solid State Sci. Technol.*, **9**, 015004 (2020).
43. H. -Y. Kim, J. W. Lee, Y. M. Moon, J. T. Oh, H. -H. Jeong, J. -O. Song, T. -Y. Seong, M. Kneissl, and H. Amano, *ECS J. Solid State Sci. Technol.*, **9**, 015014 (2020).
44. S. -K. Sinha, H. -A. Feng, C. -Y. Chung, C. -W. Tu, and R. -H. Horng, *ECS J. Solid State Sci. Technol.*, **9**, 015015 (2020).
45. H. G. Nam, M. G. Nam, P. J. Yoo, and J. -H. Kim, *Soft Matter*, **15**, 785 (2019).
46. Q. Zhang, X. Liu, L. Duan, and G. Gao, *Chem. Eng. J.*, **365**, 10 (2019).

Figure Captions

Figure 1. Schematic cross-sectional structural diagrams of the bonded and reference unbonded LED samples.

Figure 2. (a) Plane-view and (b) cross-sectional scanning microscope images of the unpolished back surface of the GaAs substrate of the LED wafer, to be bonded to the Si piece.

Figure 3. Cross-sectional scanning microscope image of the bonded interface in the fabricated III–V LED on Si.

Figure 4. Plane-view optical photographs of (a) the bonded III–V LED on Si and (b) the reference unbonded LED at a current density of 156 μA cm^{-2} (100 μA) at 25 ℃.

Figure 5. Light–voltage–current plots of the bonded III–V LED on Si and the reference unbonded LED at 25 ℃.

Figure 6. Light–current plots of the bonded III–V LED on Si at 25 ℃ (before and after the measurement at 73 ℃) and 73 ℃.

Figure 7. Luminescence spectra of the bonded III–V LED on Si and the reference unbonded LED at a current density of 781 μA cm^{-2} (500 μA) at 25 and 73 ℃.

Figure 8. Time-evolution of the output optical power of the bonded III–V LED on Si under a continuous current injection with a density of 25 μA cm^{-2} at 25 ℃. (Inset) Luminescence spectra at 0 and 102 h.

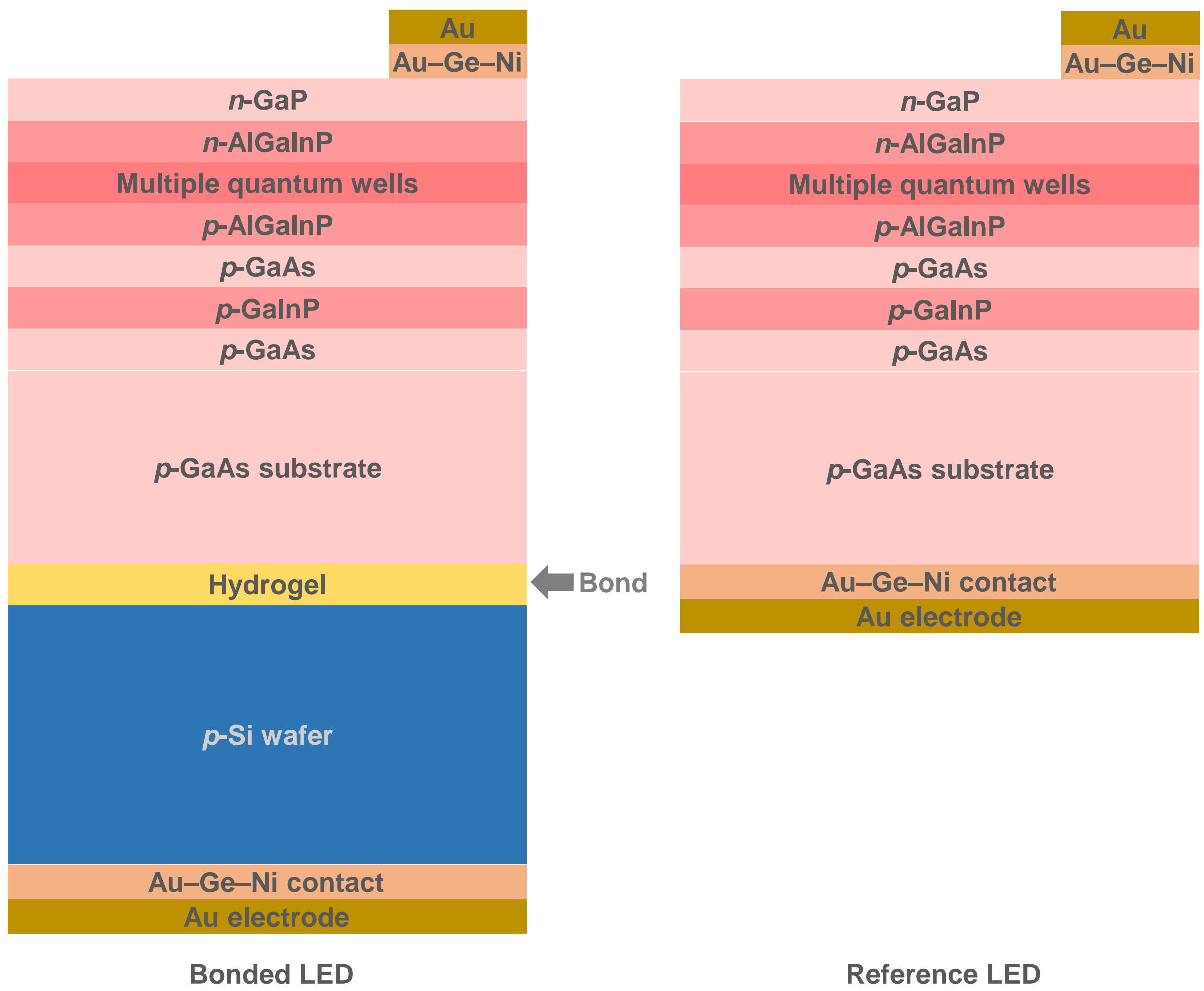

Figure 1

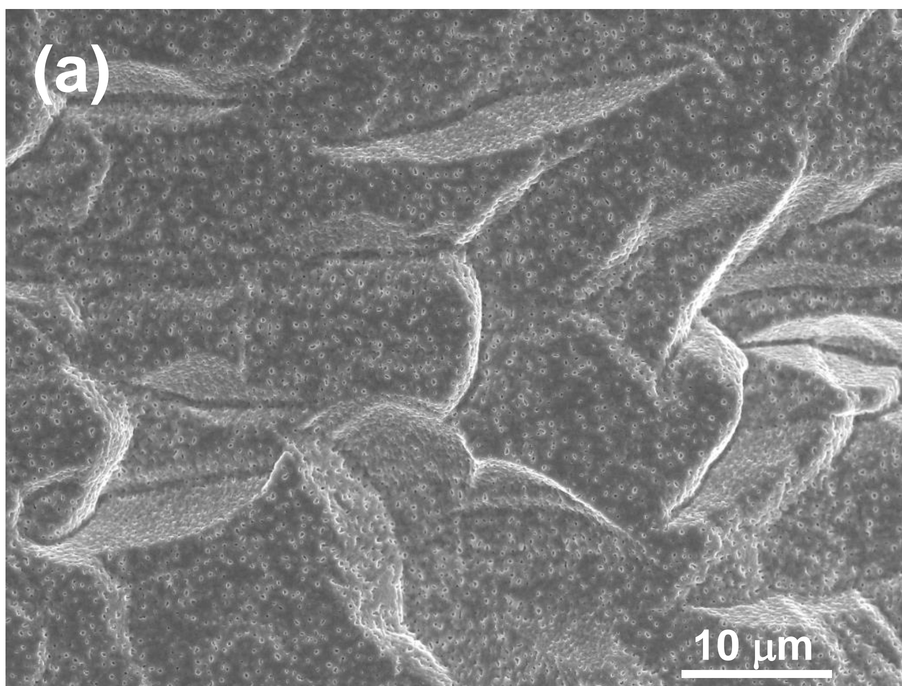

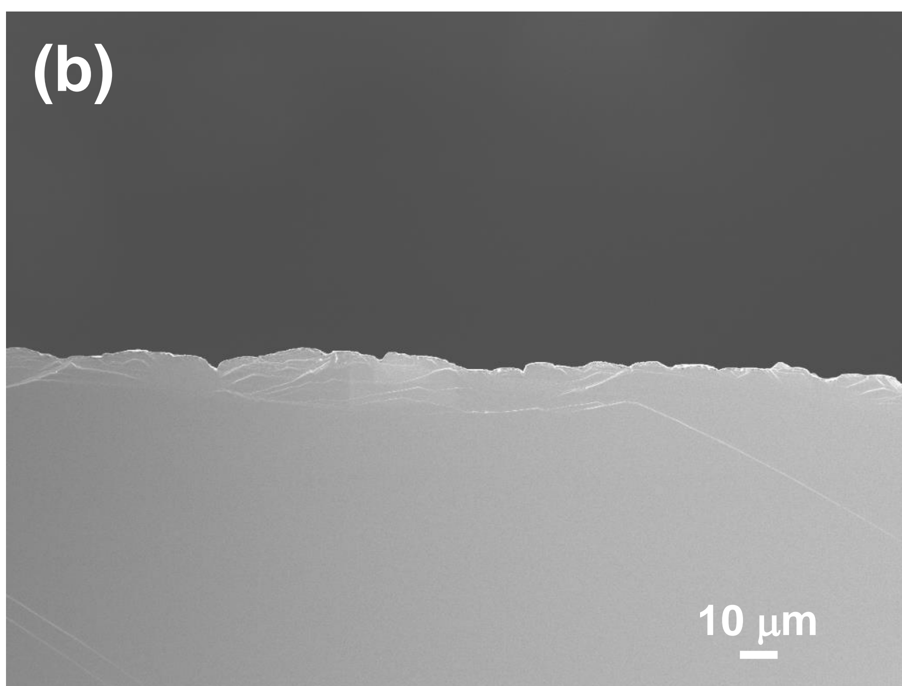

Figure 2

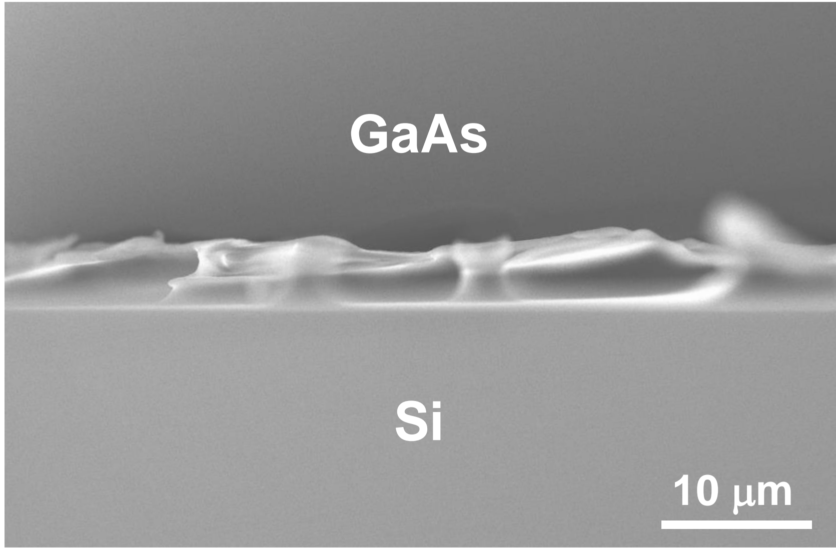

Figure 3

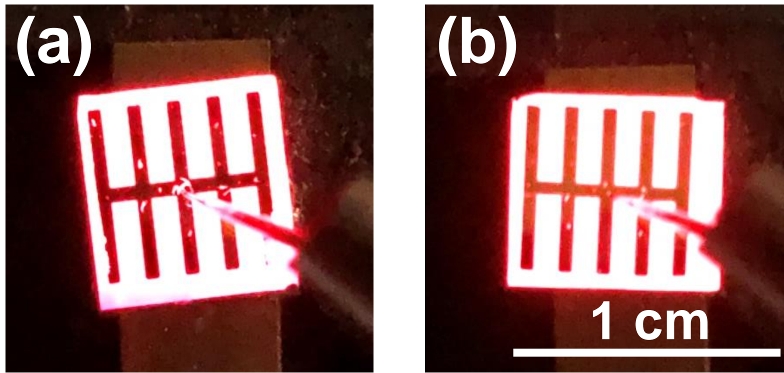

Figure 4

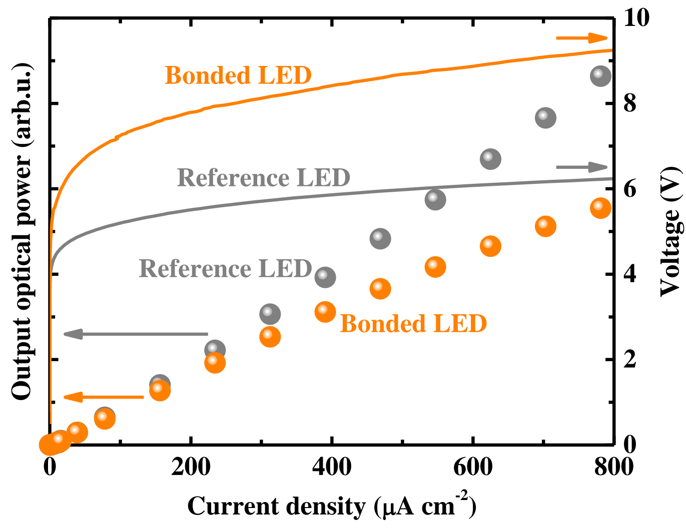

Figure 5

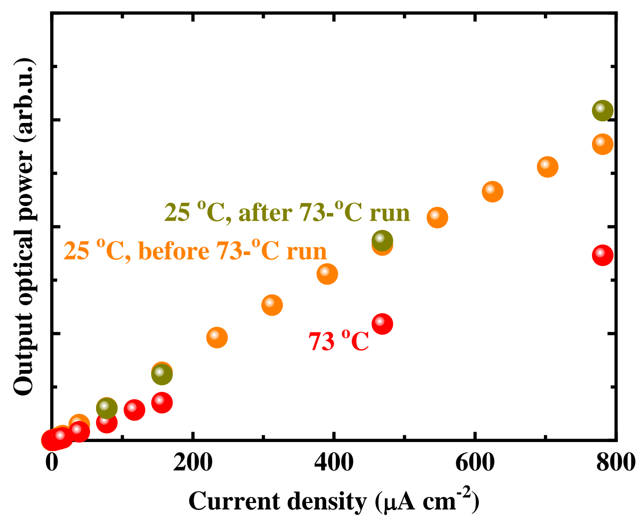

Figure 6

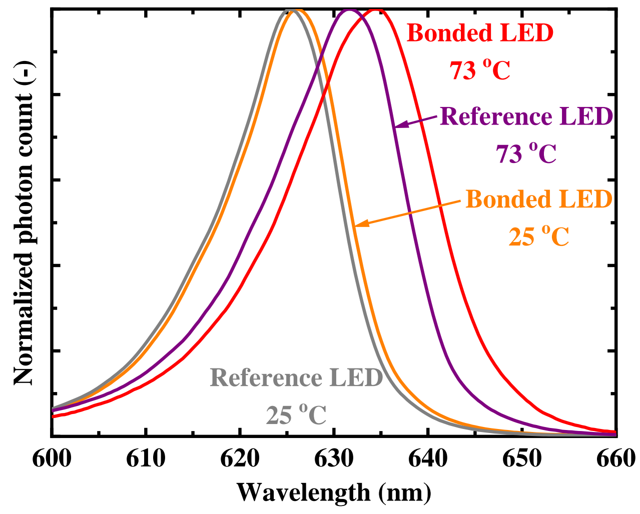

Figure 7

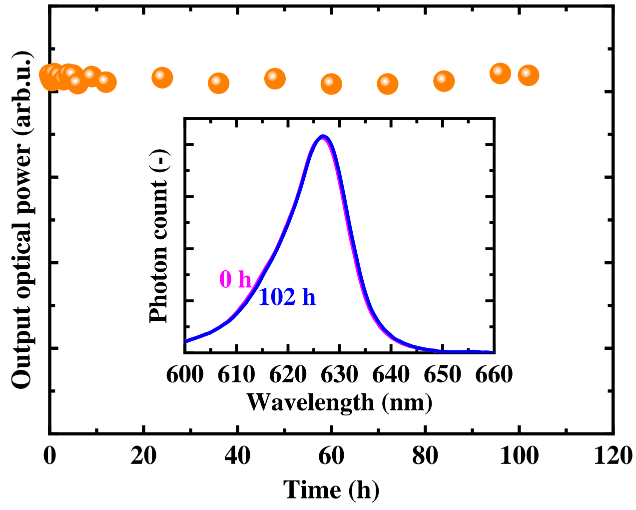

Figure 8